JOURNAL OF THERMOPHYSICS AND HEAT TRANSFER
Vol. 7, No. 2, April–June 1993

Thermal Buoyancy and Marangoni Convection in a Two Fluid Layered System

N. Ramachandran*
NASA Marshall Space Flight Center, Huntsville, Alabama 35812

Thermal buoyancy and surface tension driven convection is numerically investigated in a system with two immiscible fluids. The geometry investigated has an open cavity configuration with the lighter fluid situated on top of the heavier fluid, forming a stable layered system. The upper fluid meniscus and the interface are assumed to be flat and undeformable in the calculations. The governing equations and boundary/interface conditions are solved by a control volume-based finite difference scheme for two pairs of immiscible fluids; the water-hexadecane system and a so-called generic system. The steady-state calculations predict dramatically different flows when interfacial tension effects are included or excluded from the system model. These differences are particularly appreciable in surface tension-dominated flows, that are typical of microgravity situations. Complex flow patterns, with induced secondary flows, are noticed in both the fluids. In general, the overall system heat transfer is found to increase with increases in the thermal buoyancy and surface tension effects, but the behavior of the system flow and thermal fields is not easy to characterize when different combinations of these forces are considered.

Nomenclature

A = aspect ratio, H/L
g = acceleration due to gravity
H = height of the cavity
H_0 = height of fluid I
h = local heat transfer coefficient
k = thermal conductivity
L = length of the cavity; length scale
Ma = Marangoni number, Eqs. (19) and (20)
Nu = average Nusselt number, Eq. (23)
Nu_y = local Nusselt number, Eq. (22)
Pr = Prandtl number, (ν/α)
p = pressure
Ra = Rayleigh number, Eq. (14)
T = temperature
U, V = dimensionless velocities in the x and y directions $(/U_{ref})$
U_{ref} = velocity scale, $(\alpha/L)\ Ra^{1/2}$, (properties of fluid I)
u, v = velocity components in the x, y directions
X, Y = dimensionless Cartesian coordinates, $(/L)$
α = thermal diffusivity
β = thermal expansion coefficient
Δ = difference
θ = dimensionless temperature, Eq. (15)
μ = dynamic viscosity
ν = kinematic viscosity
ρ = density
σ = surface tension
ψ = stream function, Eq. (16)

Subscripts
f = environment conditions
i = interface conditions
I = reference to heavier fluid, fluid I
II = reference to lighter fluid, fluid II
1 = temperature suffix for hot wall
2 = temperature suffix for cold wall

Received Nov. 9, 1989; presented as Paper 90-0254 at the AIAA 28th Aerospace Sciences Meeting, Reno, NV, Jan. 8–11, 1990; revision received May 14, 1992; accepted for publication May 27, 1992.

*Associate Scientist, Universities Space Research Association. Member AIAA.

Introduction

THE study of convective heat transfer in a system with more than one fluid is of interest to several engineering applications. To cite a few, metal casting operations, crystal growth methods, and the heat transfer phenomena occurring in day-to-day processes like the presence of air pockets in heat exchangers, water layers in multiple layer glass windows, etc., involve the interaction of natural convection in immiscible fluids. The quest for making bigger and purer crystals for the electronics industry has led to adaptations and refinements of several terrestrial crystal fabrication methods to the microgravity environment of space. While the gravity effects are minimized on a space-based laboratory, surface tension effects are dominant at exposed free surfaces of a melt, and the resulting Marangoni or surface tension driven convection causes imperfections in a growing crystal. One of the ways of minimizing this Marangoni convection is the use of an encapsulant to seal off the melt-free surfaces. For example, in the Czochralski growth of Gallium Arsenide (GaAs), a liquid encapsulant like Boron trioxide, which is a high viscosity, low melting point glass, is used to reduce the surface tension driven flow and also used to prevent arsenic from evaporating and compromising the crystal stoichiometry.[1] Similarly, in the float zone crystal growth method, liquid encapsulation has been used[2] in obtaining striation-free silicon crystals in a microgravity environment. It is noted, that while the buoyancy forces are reduced in space, they are nevertheless finite and are of consequence to materials processing techniques that involve strong temperature gradients. The modeling of such processes requires the understanding of the behavior of systems composed of immiscible fluids and the interaction of the various associated forces that control the system flow and heat transfer characteristics.

Szekely and Todd[3] investigated the transient and steady-state natural convection effects in a system of immiscible liquids enclosed in a rectangular cavity, with differentially heated vertical side walls. The investigation, which was comprised of both numerical simulation and experimentation and good agreement, was reported between the two efforts. Their stable, layered system was composed of Therminol (ρ = 1.54 $\times$ 10^3 kg/m^3 and Pr = 2.5 $\times$ 10^5) and Ambiflow (ρ = 1.06 $\times$ 10^3 kg/m^3 and Pr = 1.75 x 10^4), and detailed temperature measurements were reported. Flow visualizations were, however, not performed, and the primary and secondary flow patterns were delineated from the measured temperature pro-

files. Knight and Palmer,[4] in their numerical study, simulated free convection in dissimilar fluid layers in an enclosure, and presented results for the flow and thermal fields for different Grashof numbers and different fluid heights. They reported a drop in the overall system heat transfer rate when the heavier fluid level was dropped, and the reverse effect occurred when the height of the heavier fluid was increased. They, however, reported an error calculating the system Grashof numbers, and therefore, their results did not refer to a particular set of fluids, but predicted the general trends for a generic two-fluid system. A similar numerical study was conducted by Kimura et al.[5] A detailed heat transfer correlation for natural convection from two immiscible fluids was developed by Sparrow et al.[6] based on experimental results. They obtained a single nondimensional group to correlate the system Nusselt number. Myrum et al.[7] reported detailed results from numerical simulations of free convection in a complex enclosure, for three different, immiscible fluid pairs. The effect of interfacial tension was also included in the study. The results showed no effect of interfacial tension for the air-liquid system, but some effect for the liquid-liquid case. Free convection in multiple fluid layers heated from below was examined by Simonovskii[8] and the stability of such a system was numerically investigated in Ref. 9.

The present study is aimed at investigating the natural convection phenomenon in a stable system of immiscible fluids contained in an open container. The geometry models the two-phase behavior typical of many crystal growth and materials processing techniques and is intended to provide insight into the system flow and thermal characteristics. The effect of meniscus and interfacial tension is also included in the problem formulation to study the interaction of the buoyancy and surface tension forces and their subsequent effect on the system thermofluid behavior.

Physical Setup and Governing Equations

A schematic of the geometry under investigation is shown in Fig. 1. The system consists of two immiscible fluids (water and hexadecane in the figure) contained in a two-dimensional, unit aspect ratio ($H/L = 1$) open cavity. Equal amounts of either fluid are considered ($H_0/H = \frac{1}{2}$) with the lighter fluid occupying the space on top of the heavier fluid, thus forming a stable layered system. A temperature gradient normal to the gravity vector is imposed on the system by maintaining the side walls of the cavity at different isothermal conditions. The two fluid interface and the upper fluid meniscus (free surface) are assumed to be flat and undeformable in the present calculations. In reality, the interface shape and location is dictated by the continuity of pressure, but as pointed out in Refs. 4 and 7, for a system composed of Boussinesq fluids, with $\rho_I > \rho_{II}$, this approximation can be made. In all the subsequent discussions, the terms meniscus and interface will be used to refer to the upper fluid-free surface and the two fluid interface, respectively. In the computations, the floor of the cavity and the meniscus are assumed to be thermally adiabatic in nature.

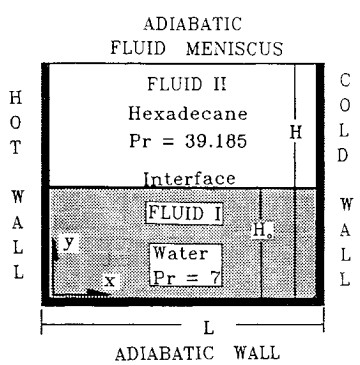

Fig. 1 Schematic of the physical setup.

The governing equations for an incompressible, Newtonian fluid written in Cartesian coordinates are as follows:

Continuity

$$u_x + v_y = 0 \tag{1}$$

Momentum

$$uu_x + vu_y = -p_x/\rho + \nu(u_{xx} + u_{yy}) \tag{2}$$

$$uv_x + vv_y = -p_y/\rho + \nu(v_{xx} + v_{yy}) + g\beta(T - T_f) \tag{3}$$

Energy

$$uT_x + vT_y = \alpha(T_{xx} + T_{yy}) \tag{4}$$

where the suffixes denote differentiation with respect to that quantity. In the above equations, all the properties are assumed constant, except for the fluid density which is modeled using the Boussinesq approximation in Eq. (3). It is noted that the governing equations are for steady-state flow and are applicable to each of the two fluids considered in the system. The boundary conditions for the problem are given below:

$$u = v = 0; \quad \text{at} \quad x = 0, x = L; \quad y = 0 \tag{5}$$

$$\mu u_y = \sigma_T T_x \quad \text{at} \quad y = H \tag{6}$$

$$T = T_1 \quad \text{at} \quad x = 0 \text{ (hot side)} \tag{7}$$

$$T = T_2 \quad \text{at} \quad x = L \text{ (cold side)} \tag{8}$$

$$T_y = 0 \quad \text{at} \quad y = 0, y = H \tag{9}$$

At the interface the following conditions are imposed:

Continuity of velocity and temperature

$$u_I = u_{II}; \qquad T_I = T_{II} \tag{10}$$

Impermeability condition

$$v_I = v_{II} = 0 \tag{11}$$

Continuity of heat flux

$$(kT_y)_{II} = (kT_y)_I \tag{12}$$

Interface force balance

$$\sigma_{Ti}T_x + (\mu u_y)_{II} = (\mu u_y)_I \tag{13}$$

where the suffix "i" represents values at the interface and the other suffixes denote differentiation. The governing equations and the boundary/interface conditions are cast into dimensionless form by introducing appropriate scale factors for length L, velocity ($U_{ref} = \alpha/LRa^{1/2}$, based on fluid I) and temperature (ΔT). Ra used in the velocity scale definition and in all subsequent discussions is defined as follows based solely on the properties of the heavier fluid:

Rayleigh number

$$Ra = (g\beta\Delta TL^3)/(\nu\alpha) \tag{14}$$

The dimensionless temperature is defined as

$$\theta = (T - T_2)/(T_1 - T_2) \tag{15}$$

and the dimensionless stream function used in presenting the flowfield behavior is defined as

Stream function

$$\rho U = \psi_Y; \qquad \rho V = -\psi_X \tag{16}$$

It may be mentioned, that the choice of the velocity scale is based on that used in natural convection calculations, the results from which were sought to be compared with those for surface tension driven flows from the present study. The meniscus and interfacial conditions [Eqs. (6) and (13)], are transformed into the following form with the introduction of the scaling factors:

Meniscus boundary condition

$$U_Y = (Ma/Ra^{1/2})\theta_X \tag{17}$$

Interface condition

$$(Ma_i/Ra^{1/2})\theta_X + (\mu_{II}/\mu_I)(U_Y)_{II} = (U_Y)_I \tag{18}$$

where Ma and Ma_i are, respectively, the meniscus and interfacial Marangoni numbers defined in the following manner:

Meniscus Marangoni number

$$Ma = \sigma_T \Delta TL/(\mu\alpha) \tag{19}$$

Interfacial Marangoni number

$$Ma_i = \sigma T_i \Delta TL/(\mu\alpha) \tag{20}$$

In Eq. (20), the property values are those of the heavier fluid (water in this case). At the interface, the force balance Eq. (13) incorporates the interfacial tension effect, with σ_{Ti} representing the gradient of interfacial tension with temperature. Similarly, at the meniscus, the surface tension effect is incorporated in the boundary condition [Eq. (6)] where σ_T refers to the gradient of surface tension of the upper fluid with temperature. To evaluate these gradients, the surface tension variations with temperature of the air-water and air-hexadecane systems, taken from Ref. 10, were plotted as shown in Fig. 2. The data were fitted with a least-squares linear fit, and their slopes were determined. For the water-hexadecane system, the surface tension values were calculated as in Ref. 7, using the Antonow rule[11] which states that "the surface tension between two liquids is equal to the difference between the σ_T values for the respective air-liquid systems." This method was used to generate the water-hexadecane curve shown in Fig. 2, and the slope of this curve was used to calculate the interfacial tension effect used in the computations. An examination of Fig. 2 reveals that for the water-hexadecane

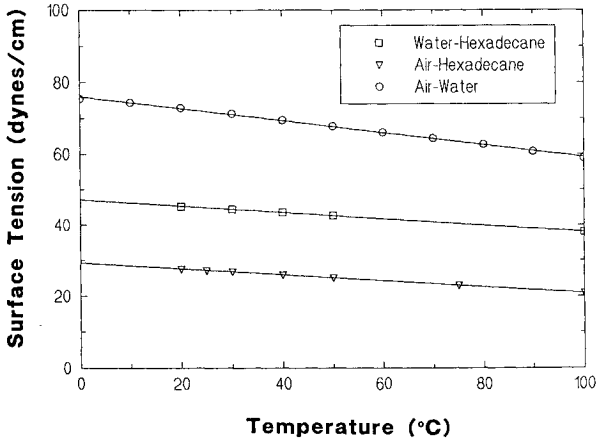

Fig. 2 Variation of surface tension with temperature.

Table 1 Water-hexadecane system (system parameters and properties) $L = H = 0.01$ m; $\Delta T = 25$°C

Property	Water	Hexadecane
μ, kg/m-s	9.8×10^{-4}	3.45×10^{-3}
ρ, kg/m^3	997.4	773.4
ν, m^2/s	9.826×10^{-7}	4.462×10^{-6}
α, m^2/s	1.449×10^{-7}	1.1387×10^{-7}
Cp, KJ/kg°C	4.179	1.651
β, /°C	2.772×10^{-4}	9.0×10^{-4}
λ, W/hr-°C	0.604	0.1454
σ_T, N/m-°C	-0.168×10^{-3}	-0.084×10^{-3}
Pr	7	39.185

Water (w)—hexadecane (h): $\mu_h/\mu_w = 3.5214$; $\rho_h/\rho_w = 0.7754$; $\beta_h/\beta_w = 3.247$; $k_h/k_w = 0.2407$; $\sigma_{Ti} = -0.0908 \times 10^{-3}$ N/m°C.

system, the presence of hexadecane tends to lower the surface tension of water (air-water system) and its gradient with temperature. This principle of lowering the surface tension force and its gradient due to the presence of a different fluid, is used in crystal growth methods like the Czochralski and the floating zone techniques to enhance the crystal purity. In these applications, strong Marangoni convection often causes strong temperature oscillations in the melt which cause striations and inhomogeneities in the grown crystal. These effects are particularly severe in a microgravity environment where the buoyancy force is small and surface tension is the dominating force influencing the thermodynamic characteristics of the melt. The minimization of the deleterious convection effects by coating the zone with a different liquid (the liquid encapsulated float zone method) or by adding an immiscible, viscous, high Prandtl number fluid (the liquid encapsulated Czochralski method) has shown to yield crystals with fewer nonuniformities.[1]

The properties of water and hexadecane[10] are tabulated in Table 1 along with the temperature gradients of surface tension determined from Fig. 2. The values of these gradients reveal that the interfacial tension gradient is approximately equal to the surface tension temperature gradient of hexadecane, and thus, the surface tension effects at the interface and at the meniscus are of approximately the same magnitude. Furthermore, since both of these gradients are negative, the Marangoni flows in these regions are both directed from the hot wall (region of lower surface tension) to the cold wall (region of higher surface tension), and therefore should assist the thermal buoyancy driven flow. However, as will be seen later, the presence of the impermeable interface tends to significantly modify the surface tension and thermal buoyancy force interactions.

As a second part of the study, a so-called generic, two-fluid, immiscible system was studied, to obtain information from a parametric variation of the Rayleigh number and the meniscus and interfacial Marangoni numbers. For this generic model, the system properties were chosen so that the Pr of the lighter fluid II was twice that of the denser fluid I ($Pr = 1$), and both the fluids had the same dynamic viscosities. The other property ratios of the system were as follows:

$$k_{II}/k_I = 0.5; \quad \rho_{II}/\rho_I = 0.8; \quad \beta_{II}/\beta_I = 2.0 \tag{21}$$

The physical quantities of interest determining the system heat transfer are the local and average Nusselt numbers which are given by the following expressions:

Local Nusselt number

$$Nu_y = hL/k = -\theta_X|_{\text{wall}} \tag{22}$$

Average Nusselt number

$$Nu = \int_0^H Nu_y \, dY \tag{23}$$

In the subsequent sections, results for the water-hexadecane system will be discussed first, followed by discussions of the results for the generic system.

Method of Solution

The governing equations and boundary conditions [Eqs. (1–9)] were solved in the primitive variables using an implicit control volume finite difference method[12] using the SIMPLE-C velocity-pressure correction algorithm. The code is set up in a generalized body-fitted coordinate system and utilizes grid staggering between the velocity vectors and scalar (pressure) nodes to ensure the numerical stability of the solutions. Grid dependency was gauged by computing natural convection of a water-hexadecane system contained in an open cavity. Both meniscus and interfacial tension effects were incorporated in the calculations. A summary of the results obtained from this exercise are provided in Table 2. The second and third columns in the table are the grid dimensions in the X and Y directions, respectively, in the corner regions (singular points) of the computational domain. The results show that the inadequate resolution of these regions, where steep temperature gradients are encountered, can lead to erroneous results. An 81 × 80 (X,Y) staggered grid was adopted for all the cases that were simulated in this study. A typical grid distribution used in the computations is shown in Fig. 3. The solution procedure consists of the following sequence of events: 1) provide an initial guess for the velocity, pressure, and temperature fields, 2) solve the velocity fields, 3) solve the temperature field, 4) solve the pressure correction equation, and 5) correct the velocity and pressure fields and return to step 2 until convergence is obtained. In the numerical scheme, the convective terms were approximated using positive coefficient skew upwind differencing and the diffusion terms were approximated by the central differencing scheme. These differencing methods have been shown[13] to be cost effective, accurate, and to have reduced numerical diffusion compared to the conventional upwinding methods. The adiabatic boundary conditions at the meniscus and the container bottom wall, as well as the interface conditions, were approximated by first-order differences and, therefore, only involved the grid points that are in the immediate vicinity of these regions. The solution procedure is iterative with the whole domain being swept during each iteration, followed by an update of the interfacial velocity and temperature quantities [Eqs. (10–13)]. Only steady-state solutions were sought for all the cases that were investigated, and an error criteria of 10^{-4} was imposed for the sum of the normalized residuals of the momentum, pressure correction, and energy equations.

Table 2 Grid dependence study, water-hexadecane system—*Ma* and Ma_i included

Grid, (X,Y)	ΔX, Corner	ΔY, Corner	Nu	ψ_{max}	ψ_{min}
31 × 40	0.0115	0.0078	14.46	0.0161	−0.0615
41 × 60	0.0115	0.0078	14.00	0.0167	−0.0601
51 × 60	0.0091	0.0078	13.64	0.0170	−0.0580
81 × 80	0.0038	0.0041	11.61	0.0178	−0.0572
101 × 100	0.0031	0.0032	11.41	0.0177	−0.0580

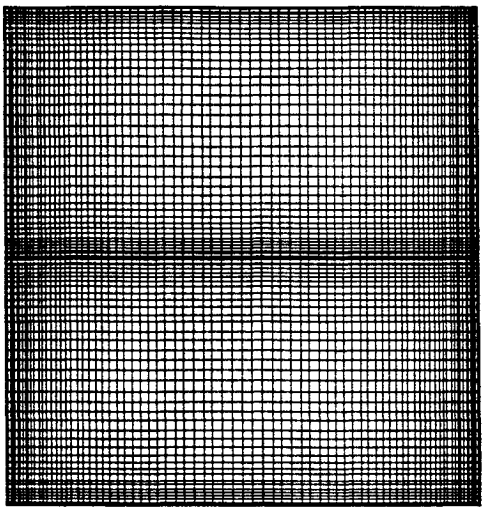

Fig. 3 80 × 81 Grid distribution used in the computations.

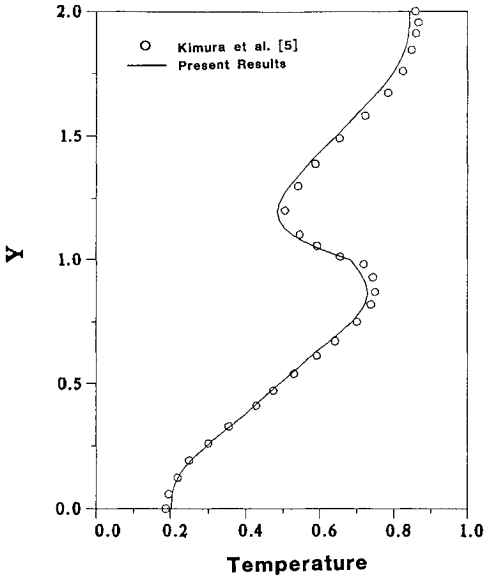

Fig. 4 Code validation. Comparison of results with Kimura et al.[5]

In order to validate the code, a test problem taken from Kimura et al.[5] (case 1 in their paper) was numerically simulated. Figure 4 shows the excellent agreement between the present calculations and those reported in Ref. 5.

Results and Discussion

Water—Hexadecane System

As a first step in the numerical simulations, the classical problem of natural convection in an enclosure is calculated. For this problem, there is no meniscus and the two-fluid system is bounded by no slip walls on all four sides. The interface is treated as an impermeable shear layer and no surface tension effects are considered. The calculations were done for a 1 × 1 cm container with a temperature difference of 25°C imposed between the hot (left) and the cold (right) walls. For the water-hexadecane system, this corresponds to $Ra = 4.9 \times 10^5$ based on the property values given in Table 1.

The steady-state stream function and isotherm distributions for this case are shown in Fig. 5. Two large recirculations, one in each fluid, are seen in the system. Both the cells are driven in the clockwise (CW) direction by thermal buoyancy and this causes a conflict situation in the vicinity of the interface. The stronger hexadecane cell drives a small counterclockwise (CCW) cell in the water column. For the present set of heating conditions, the thermal buoyancy force in hexadecane is about three times stronger than that in water (due to differences in the thermal expansion coefficient) and, hence, causes the small secondary circulation in water. The results of Knight and Palmer[4] also showed similar flow patterns with the upper fluid driving a secondary circulation in the lower fluid. For the air-water system examined in Ref. 4 this behavior is more pronounced, because the thermal coefficient of expansion of air is 15 times that of water and causes a much stronger circulation cell in air than in water. The isotherm distribution in Fig. 5 shows significant distortion and this behavior is typical of strong convection effects in high Pr fluids. The temperature field also shows that the grid used for spatial discretization is adequate to resolve the thermal boundary

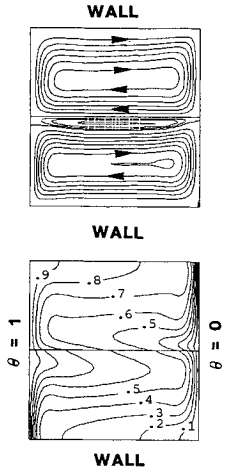

Fig. 5 Stream function and isotherm plots; enclosure problem, $Ma_i = 0$, case 1.

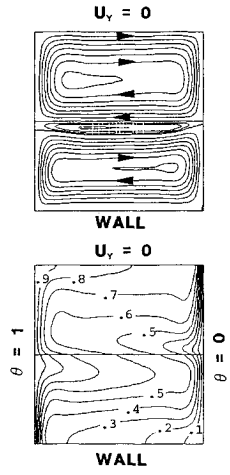

Fig. 6 Stream function and isotherm plots; open cavity, $Ma = Ma_i = 0$; (reference) case 2.

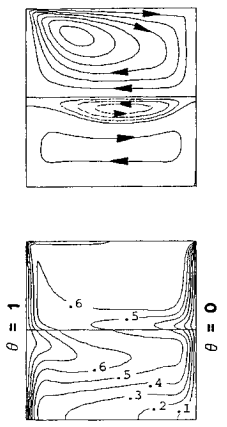

Fig. 7 Stream function and isotherm plots; open cavity, $Ma = -5.343 \times 10^4$; $Ma_i = 0$, case 3.

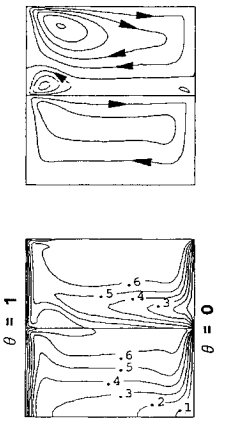

Fig. 8 Stream function and isotherm plots; open cavity, $Ma = -5.343 \times 10^4$; $Ma_i = -1.6 \times 10^5$, case 4.

layers in both the fluids. The calculated average Nusselt number was the same for both the hot and cold walls (true for all cases investigated in the study) and is equal to 5.583 for this case. The system parameters and the maximum stream function value for the water-hexadecane system are tabulated in Table 3 for the different cases that were computed. Also included in the table are the average Nusselt number and the maximum values of the "u" velocity at the meniscus and the interface.

Figure 6 shows the streamlines and isotherms for case 2, where a meniscus is present in hexadecane and the other conditions are the same as in case 1. In the calculations, the meniscus is treated as a zero shear surface ($U_y = 0$) and no surface tension effects are included. The flow and thermal fields for cases 1 and 2 look similar and only minor differences are noticed between the two cases. The maximum stream function value $|\psi_{max}|$ characterizing the strength of the primary circulations, is approximately 3% larger than the previous case, and the average Nusselt number ($Nu = 5.817$) is about 4% larger than that for the enclosure problem. In the stream function plot, the center of the cell in hexadecane is also shifted slightly upwards in case 2 than in case 1, due to the absence of the restraining wall. The maximum velocity at the meniscus is 1.27 mm/s and that at the interface is 1.19 mm/s. In the ensuing discussions, case 2 with the no shear boundary condition at the meniscus, will be referred to as the reference case and will be used for comparing results with the other cases.

Calculations were repeated with surface tension effects included at the fluid meniscus for case 3 [$Ma = -5.343 \times 10^4$ based on Eq. (19) and properties from Table 1]. Results for this case are presented in Fig. 7. The flowfield shows the dominating effect of Marangoni convection, with a strong CW circulation in hexadecane that drives a fairly large cell in water. This shear cell extends to a height of about $\frac{1}{3}H_0$, and is strongest near the cavity centerline. The isotherms show strong boundary-layer buildup in hexadecane along both the side walls and also disclose the existence of an isothermal core ($\theta = 0.6$) in hexadecane. The average Nusselt number for this case is 34% larger than that for the reference case, and the maximum velocity at the meniscus is two orders of magnitude larger than that in the reference case, as shown in Table 3.

In case 4, the effect of interface tension is also included in the computations and the other parameters are held the same as in case 3. The interfacial Marangoni number ($Ma_i = -1.6 \times 10^5$) is larger than the Ma value at the meniscus, and tends to drive the fluid (water) from the hot side to the cold side, thus complementing the thermal buoyancy driven flow in water. Results from the calculations which are presented in Fig. 8 show a dramatic change in the flow behavior for the present case. This behavior is markedly different from case 3 where hexadecane caused a secondary recirculation in water. In the experimental work,[3] secondary flow was reported in the upper fluid and not in the lower fluid, a trend that conforms with the present findings. However, as mentioned in the introduction, they used very viscous fluids with low thermal conductivities and a direct, quantitative comparison cannot be made with their results. The interfacial tension effects are seen to be critical to the problem. The predicted flow behavior can be totally incorrect if the interfacial tension effect is not included in the problem formulation. It should be stated at this point that the meniscus or interface deformation was not

Table 3 Water—hexadecane system, $Pr_I = 7$; $Pr_{II} = 39.185$; $Ra = 4.9 \times 10^5$

Case no.	Top boundary condition	Ma	Ma_i	Nu	$\lvert\psi_{max}\rvert$	$\lvert u_{max}\rvert_{int}$, cm/s	$\lvert u_{max}\rvert_{top}$, cm/s
1	Wall	0	0	5.583	0.0142	0.1187	0.0
2	$U_y = 0$	0	0	5.817	0.0146	0.1187	0.1267
3	Ma	-5.343×10^4	0	7.817	0.0646	0.2686	25.256
4	Ma	-5.343×10^4	-1.6×10^5	11.61	0.0572	13.460	24.316

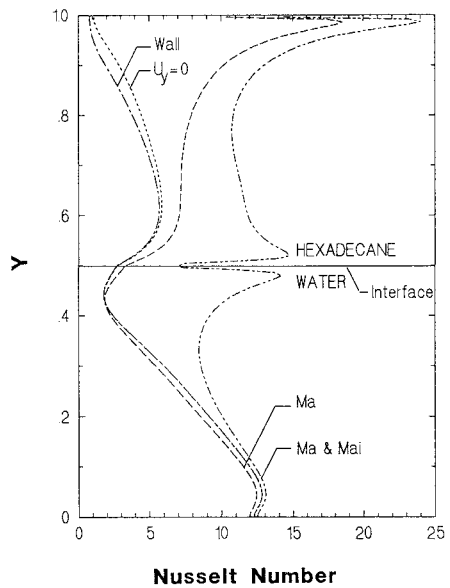

Fig. 9 Local Nusselt number distribution for the hot wall; water-hexadecane system.

considered in this study and this factor might prove to be another important issue yet to be investigated. The average Nusselt number for this case is twice as large as the reference case and about 50% greater than for case 3. The heat transfer correlation of Sparrow et al.[6] can be used to predict the average system Nusselt number. The correlation equation yields a Nusselt number of 9.52 compared to 11.61 obtained from the calculations; a difference of approximately 20%. The Nusselt number calculated without the interfacial tension is 7.817. It appears that the estimate of the interfacial tension accounts for this variation to a large degree. Other reasons for this difference in heat transfer are a matter of conjecture, pending further calculations to resolve the issue.

The local Nusselt number distribution along the hot wall, for the four cases discussed above, are shown in Fig. 9. The following inferences can be drawn from the plots.

For the enclosure problem (case 1), the maximum local heat transfer rate is located in water near the container bottom wall. For case 2, the Nu_y behavior in water is identical to the previous case and a slight enhancement in the local heat transfer rate is observed in hexadecane. Since the only modification for case 2 from case 1 is the absence of the no-slip wall, the flow is stronger near the meniscus for this case and contributes to this overall augmentation of the Nusselt number in hexadecane. The plot also shows that the free surface effects start diminishing with increasing distance from the meniscus in fluid II and are not felt in the lower fluid. In both cases 1 and 2, the characteristic "S" shape of the plots and the isotherm profiles (Figs. 5 and 6), indicate the presence of two major recirculation cells. Although a secondary cell is present in water for this case, this circulation is feeble and has little impact in modifying the local heat transfer characteristics of the system.

In case 3, the strong Marangoni convection at the meniscus dominates the flowfield and causes significant heat transfer enhancement in hexadecane. This flow causes a local peak in Nu_y near the upper fluid meniscus. The heat transfer in water, on the other hand, is reduced due to flow deceleration by the vigorous, induced secondary flow, that opposes the primary buoyancy driven cell. Thus, the local Nusselt number in the primary circulation region of water falls below that for the reference case. However, in the vicinity of the interface, the secondary circulation promotes local heat transfer.

When both Ma and Ma_i are included in the numerical model (case 4), a second peak in Nu_y is observed in water near the interface. This boost in Nu is caused by the strong Marangoni flow due to Ma_i at the interface, and is similar to the peak near the meniscus for this and the previous cases. The Nu_y curve for case 4 shows increased heat transfer in both the liquids and yields the highest overall system heat transfer among the cases investigated.

In all 4 cases considered, the local Nusselt number in hexadecane is always increased with the introduction of additional boundary and interface conditions. For water, however, the Nu behavior is not as monotonic with no effect seen in case 2 over case 1, a decrease for case 3 and a subsequent increase for case 4. Therefore, the per fluid heat transfer rates show different trends for the system parameters that were studied.

Generic System

Results for the generic system are presented in the following sections. Calculations were carried out for $Ra = 10^3$, 10^4, and 10^5 for different combinations of Ma and Ma_i. Table 4 lists the various cases that were simulated and some relevant results from the computations. Again, as in the previous section, the reference case consists of the open cavity problem with a no shear meniscus and no interfacial tension effects.

A sampling of the results for $Ma = -10^3$ and $Ma_i = 0$ are presented in Fig. 10 for three different Rayleigh numbers. For the three cases shown in the figure, the interface tension is taken as zero, and the flow is driven by the meniscus surface tension force and the thermal buoyancy force within the cavity. The stream function and isotherm plots correspond to cases 7, 14, and 21, respectively, in Table 4 and the following inferences can be drawn from the figure.

1) Case 7 corresponds to $Ra = 10^3$ and $Ma = -10^3$. For this combination, the Marangoni convection is very strong in fluid II and forms a single recirculation cell. The shear transfer across the interface causes a secondary cell in fluid I, which occupies almost the entire volume of the denser phase. The thermal buoyancy driven flow in fluid I causes relatively feeble CW cells that are confined to the cavity corners. The isotherms in the lower fluid are distorted slightly from the conduction profile, but those in the upper fluid are more strongly affected by the flowfield.

2) When Ra is increased to 10^4 (case 14), the remnants of natural convection in fluid I, seen in case 7, are strengthened and a fuller CW cell is formed. The secondary circulation is now relegated to a small region near the interface, and the stream function values in Table 4 (ψ_{max}) indicate that it is significantly reduced in strength. The isotherms echo the flowfield and the characteristic S profiles due to the primary recirculation in fluid I are observed. The average Nusselt number is now 15.8% greater than for case 7.

3) For a further increase in Ra to 10^5 (case 21), the figure shows that the two primary circulations are now of about equal strength. Some pockets of secondary circulations are still present in fluid I, but these are confined to a very narrow area

Table 4 Generic system, $Pr_I = 1$; $Pr_{II} = 2$

Case no.	Top boundary condition	Ra	Ma	Ma_i	Nu	ψ_{max}	ψ_{min}	$\lvert U_{max}\rvert_{int}$	$\lvert U_{max}\rvert_{top}$
5	$U_y = 0$	10^3	0	0	1.039	1.55E-3	−1.64E-2	0.0565	0.1465
6	Ma		-10^2	0	1.167	3.68E-3	−2.96E-2	0.0971	0.4099
7			-10^3	0	1.918	1.47E-2	−8.66E-2	0.2840	3.3430
8			-10^4	0	4.388	1.44E-1	−5.98E-1	2.3580	66.730
9			-10^4	-10^4	6.348	2.25E-1	−3.48E-1	22.080	70.710
10			-10^3	-10^4	4.863	2.67E-1	−3.84E-1	22.840	1.6280
11			-10^2	-10^4	5.199	4.13E-1	−4.32E-1	21.810	2.5710
12	$U_y = 0$	10^4	0	0	1.756	8.29E-4	−2.24E-2	0.0589	0.2018
13	Ma		-10^2	0	1.821	9.09E-4	−2.36E-2	0.0617	0.2346
14			-10^3	0	2.221	1.62E-3	−3.37E-2	0.0848	1.2130
15			-10^4	0	4.249	3.98E-2	−1.89E-1	0.7259	21.210
16			-10^4	-10^4	6.414	7.17E-2	−1.11E-1	6.8750	22.580
17			-10^3	-10^4	4.848	8.15E-2	−1.19E-1	7.3060	0.5146
18			-10^2	-10^4	5.045	1.28E-1	−1.35E-1	6.9110	0.7537
19	$U_y = 0$	10^5	0	0	4.276	3.44E-4	−1.77E-2	0.0514	0.1866
20	Ma		-10^2	0	4.295	3.47E-4	−1.78E-2	0.0517	0.1947
21			-10^3	0	4.422	3.87E-4	−1.89E-2	0.0541	0.5119
22			-10^4	0	5.029	2.79E-3	−4.64E-2	0.1595	8.0880
23			-10^4	-10^4	7.005	2.03E-2	−3.44E-2	1.9750	7.5240
24			-10^3	-10^4	6.231	1.92E-2	−3.28E-2	2.1040	0.4322
25			-10^2	-10^4	6.049	1.88E-2	−3.26E-2	2.1160	0.1747

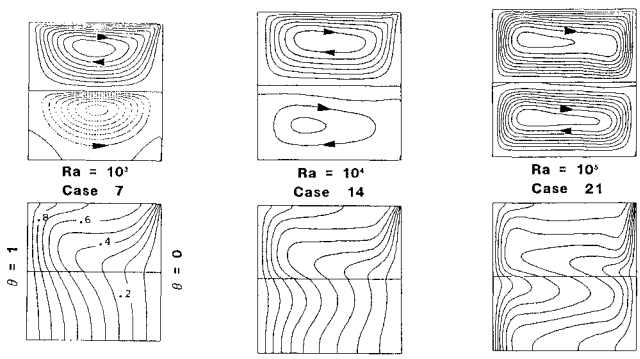

Fig. 10 Flow and thermal fields; the generic system, $Ma = -10^3$, $Ma_i = 0$.

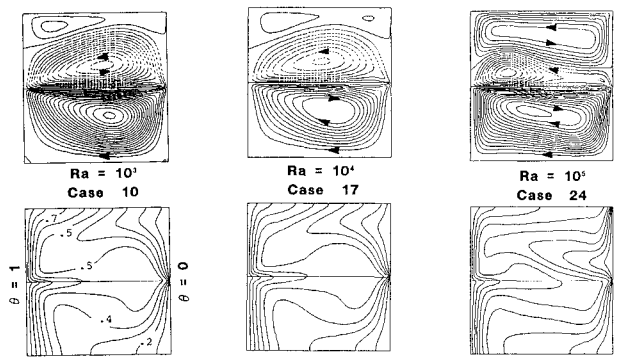

Fig. 11 Flow and thermal fields; the generic system, $Ma = -10^3$, $Ma_i = -10^4$.

adjacent to the interface. The isotherms are drawn by the flows in both the fluids, and boundary layers are evident near the side walls. The overall heat transfer increases significantly with $Nu = 4.422$ as compared to 2.221 for case 14.

The results show that, notwithstanding the complex interactions between the buoyancy and surface tension forces, with waxing and waning primary and secondary flows, the average system heat transfer is always augmented by increasing the Rayleigh number. The per fluid heat transfer rate, however, may not show this monotonic increase, and can be affected by the induced secondary flows.

Results from cases 10, 17, and 24 which consider both the meniscus and interfacial tensions, are now considered and presented in Fig. 11 for three values of the Rayleigh number ($Ra = 10^3$, 10^4, and 10^5). The meniscus Marangoni number is held fixed at -10^3 and the interfacial tension is given by $Ma_i = -10^4$. As in case 4 (water-hexadecane system), the introduction of interfacial tension results in a strong CW cell in fluid I that now drives a secondary cell in fluid II and for $Ra = 10^3$, occupies almost the entire height of fluid II. The effect of Ma_i is clearly brought out by a comparison of the flowfields for cases 10 and 7 shown in Figs. 11 and 10, respectively. Markedly different primary and secondary flow patterns are observed for these two cases that clearly point to the importance of including the surface tension effects at the two-fluid interface. The thermal fields for cases 7 and 10 also show vast differences. The average Nusselt number for case 10 is 4.863, that is 1.5 times greater than the Nu for case 7. When Ra is increased to 10^4, the secondary circulation in fluid II is diminished due to the enhanced buoyancy force, but the flowfield is still different than the computed flow behavior without the Ma_i effects (case 14 in Fig. 10). For a further increase in Ra to 10^5, the secondary circulation in fluid II is further weakened by stronger circulation in the upper fluid. The average Nusselt number for this case is 6.231, that is still 41% larger than with no Ma_i effects. From the trends seen in Figs. 10 and 11, it appears that as Ra is increased, the flow and thermal fields will tend to display similar characteristics for the cases with and without interfacial tension effects. However, for the calculations shown here ($Ra = 10^5$), the flow patterns for these two cases are still substantially different. As the strength of the thermal buoyancy force is increased, the flows will become more and more buoyancy dominated and the surface tension forces will no longer play an important role in determining the system flow and heat transfer characteristics. On the other hand, when Ra is small, surface tension is prominent and causes significant changes in the system thermofluid behavior. In these surface tension dominated flows, the interfacial tension effects are found to be very important, and strikingly different flow patterns are predicted when Ma_i is included or excluded in the model.

The average Nusselt number variation with Ra is plotted in Fig. 12 for cases with and without the interfacial tension effects. Also included in the figure is the Nu variation for the reference case. Inferences from the figure are listed below:

1) For all the cases, the average Nusselt number is larger than the corresponding reference case.

2) As Ma increases with $Ma_i = 0$ (solid lines), the average system heat transfer also increases. This behavior is also true when Ma_i is included in the computations (dashed lines).

3) The inclusion of Ma_i in the model causes enhanced heat transfer for Ma values of -10^2 and -10^3, and a slight re-

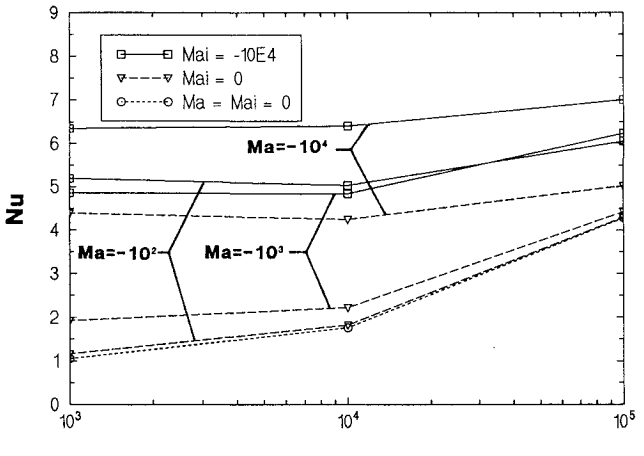

Fig. 12 Average Nusselt number variation; generic system.

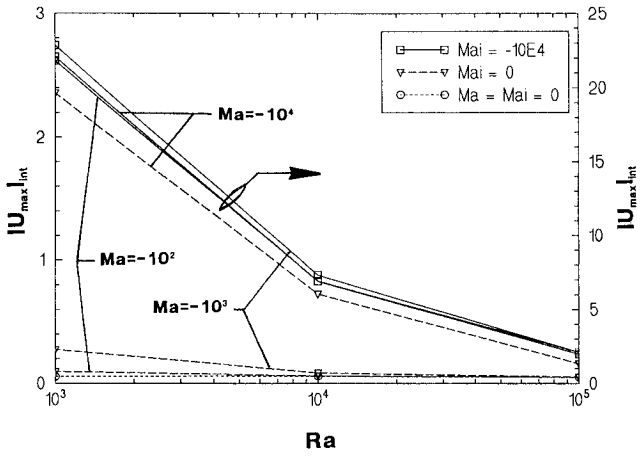

Fig. 13 Interface U velocity variation with Ra; generic system.

duction in heat transfer for $Ma = -10^4$ in comparison to the cases when Ma_i effects are not included. This reduction of heat transfer for $Ma = -10^4$, however, vanishes as Ra is increased, and eventually an increase is noticed.

4) When the flow is dominated by thermal buoyancy ($Ra = 10^5$), the effect of interfacial tension becomes smaller and the curves should approach the reference case curve as Ra is increased further. For further increases in Ra, however, the flow can undergo transition followed by the onset of turbulent flow.

The maximum interface U velocities are plotted in Fig. 13 as a function of Ra. Results from the reference cases are also drawn in the figure. It is to be noted, that as only the absolute values of U are plotted, these velocities could be generated by either primary or secondary cells at the interface. As in the Nu plot (Fig. 12), the interface velocities are found to always be larger than those observed in the reference case. For a fixed value for Ra, these velocities are found to generally increase with an increase in the meniscus Ma value; but for a fixed value of Ma, they decrease with increasing values of Ra. The velocity values with interfacial tension effects are an order of magnitude larger than those without these effects. Further, as the value of Ra is increased, all the curves tend to converge together. As mentioned earlier, higher values of Ra imply buoyancy dominated flows, and this trend in the velocity profiles is to be expected, since the velocities are nondimensionalized with the natural convection velocity scale U_{ref}. The differences between the velocities for the cases when Ma_i is included or excluded from the calculations, also become smaller as Ra increases due to the diminishing effects of surface tension. This again reinforces the fact that the interfacial tension effects are less important in buoyancy dominated flows.

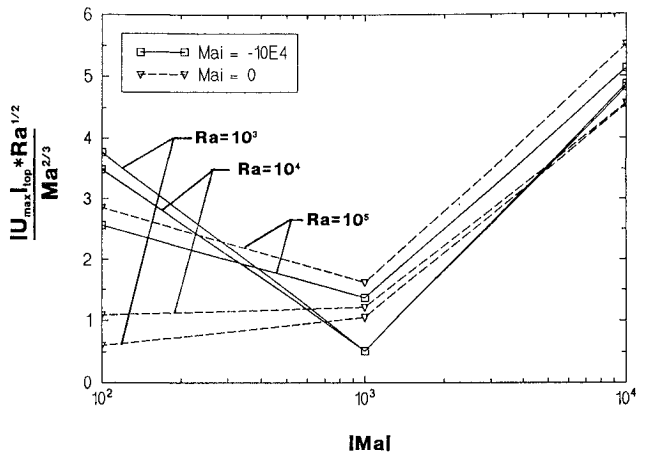

Fig. 14 Meniscus U velocity variation with Ma; generic system.

The results of Myrum et al.[7] also showed similar trends for the water-hexadecane system in a more complex physical setup. Their Ra values were about 5×10^5.

The maximum, meniscus U velocities are plotted in Fig. 14 as a function of the meniscus Marangoni number for three different Rayleigh numbers. In this figure, the U velocities are scaled with $Ma^{2/3}$ as the scaling factor. In their study of buoyancy and thermocapillary flows in shallow open cavities, Hadid and Roux[14] used $Re_M^{2/3}$ (where $Re_M = Ma/Pr$ is the surface tension Reynolds number) as the velocity scale factor and showed that the surface velocity approaches the $Ra = 0$ (only Marangoni convection) curve asymptotically, beyond a certain critical value of Re_M. The surface velocities in Fig. 14 also seem to show this asymptotic approach, as Ma is increased, and the flows become more surface tension dominated, but the trends are not very clear.

Conclusions

The interaction of thermal buoyancy and surface tension forces, in a system of two immiscible fluids, has been numerically investigated. Results from the simulations for the water-hexadecane and the generic systems show that significantly different flows can result if the interfacial tension effects are not included in the numerical calculations. These differences are particularly dramatic when the thermal buoyancy forces are small (as in a microgravity environment) and the surface tension forces are the dominating influence on the system. Complex interactions occur between the thermal buoyancy force and the meniscus and interfacial tension forces, resulting in secondary flows in both the fluids. The flowfields affect the temperature distributions within the container, thereby causing considerable variations in the local and average system heat transfer. For example, the average Nusselt number for $Ra = 10^3$, $Ma = -10^3$ is 2.5 times larger when $Ma_i = -10^4$ is included in the computations, than for the case with $Ma_i = 0$. However, as the flows become more and more buoyancy dominated, the interfacial tension effects begin to weaken and therefore are of less consequence in modifying the system flow and thermal characteristics.

References

[1]Barocela, E., and Jalilevand, A., "Liquid Encapsulated Float Zone Method for Microgravity Production of Gallium Arsenide," AIAA 25th Aerospace Sciences Meeting, AIAA Paper 87-0390, Reno, NV, 1987.

[2]Eyer, A., and Leiste, H., "Striation-Free Silicon Crystals by Floating-Zone with Surface Coated Melt," *Journal of Crystal Growth*, Vol. 71, No. 1, 1985, pp. 249–252.

[3]Szekely, J., and Todd, R. M., "Natural Convection in a Rectangular Cavity: Transient Behavior and Two Phase Systems in Laminar

Flow," *International Journal of Heat and Mass Transfer*, Vol. 14, 1971, pp. 467–482.

[4]Knight, R. W., and Palmer, M. E., "Simulation of Free Convection in Multiple Fluid Layers in an Enclosure by Finite Differences," *Numerical Properties and Methodologies in Heat Transfer*, edited by T. M. Shih, Hemisphere, Washington, DC, 1983, pp. 305–319.

[5]Kimura, T., Heya, N., Takeuchi, M., and Isomi, H., "Natural Convection in an Enclosure with Stratified Fluids" (in Japanese), *Transactions of the Japanese Society of Mechanical Engineering*, 1985, pp. 1251–1259.

[6]Sparrow, E. M., Azevedo, L. F. A., and Prata, A. T., "Two-Fluid and Single-Fluid Natural Convection Heat Transfer in an Enclosure," *Journal of Heat Transfer*, Vol. 108, No. 51, 1986, pp. 848–852.

[7]Myrum, T. A., Sparrow, E. M., and Prata, A. T., "Numerical Solutions for Natural Convection in a Complex Enclosed Space Containing Either Air-Liquid or Liquid-Liquid Layers," *Numerical Heat Transfer*, Vol. 10, Nov. 1986, pp. 19–43.

[8]Simonovskii, I. B., "Numerical Investigation of Convection in a System of Two Immiscible Fluids Heated from Below," *Izvestiya Urali'skii Nauchonyi Tsentr*, Akad. Nauk USSR, Sverdlovsk, USSR, 1979, pp. 126–131.

[9]Bourde, G. I., and Simonovskii, I. B., "Determination of Equilibrium Boundaries of a Two-Layered Convection Instability," *Journal of Applied Mathematics and Mechanics*, Vol. 43, 1979, pp. 1091–1097.

[10]Vargaftik, N. B., *Tables on Thermophysical Properties of Liquids and Gases*, Hemisphere, Washington, DC, 1975.

[11]Bikerman, J. J., *Physical Surfaces*, Academic Press, New York, 1970.

[12]Patankar, S. V., *Numerical Heat Transfer and Fluid Flow*, McGraw-Hill, New York, 1980.

[13]Syed, S., Gosman, A., and Peric, M., "Assessment of Discretization Schemes to Reduce Numerical Diffusion in the Calculation of Complex Flows," AIAA 23rd Aerospace Sciences Meeting, AIAA Paper 85–0441, Reno, NV, 1985.

[14]Hadid, B. H., and Roux, B., "Buoyancy and Thermocapillary Driven Flows in Shallow Open Cavities," *Proceedings of Conference on Finite Element Methods in Fluids*, Univ. of Alabama, Huntsville, AL, 1989, pp. 420–427.